RSC Advances

PAPER

View Article Online
View Journal | View Issue

Cite this: *RSC Adv.*, 2022, **12**, 11574

Highly stretchable, self-healing and conductive silk fibroin-based double network gels *via* a sonication-induced and self-emulsifying green procedure†

Tao Fang, Jingxin Zhu, * Shuai Xu, Lan Jia and Yanlong Ma

Regenerated silk fibroin (RSF)-based hydrogels are promising biomedical materials due to their biocompatibility and biodegradability. However, the weak mechanical properties and lack of functionality limit their practical applications. Here, we developed a tough and conductive RSF-based double network (DN) gel, consisting of a sonication-induced β-sheet physically crosslinked RSF/S gel as the first network and a hydrophobically associated polyacrylamide/stearyl methacrylate (PAAm/C18) gel as the second network. In particular, the cross-linking points of the second network were micelles formed by emulsifying the hydrophobic monomer (C18M) with a natural SF- capryl glucoside co-surfactant. The reversible dynamic bonds in the DN provided good self-healing ability and an effective dissipative energy mechanism for the DN hydrogel, while the addition of calcium ions improved the self-healing ability and electrical conductivity of the hydrogel. Under optimal conditions, the RSF/S-PAAm/C18 DN gels exhibited large extensibility (1400%), high tensile strength (0.3 MPa), satisfactory self-healing capability (90%) and electrical conductivity (0.12 $S \cdot m^{-1}$). The full physically interacted DN hydrogels are expected to be applied in various fields such as tissue engineering, biosensors and artificial electronic skin.

Received 13th February 2022
Accepted 7th April 2022

DOI: 10.1039/d2ra00954d

rsc.li/rsc-advances

Introduction

Hydrogels as soft and smart materials have received considerable attention for use in tissue engineering, drug release, sensors, and actuators.[1,2]. Regenerated Silk fibroin (RSF) derived from *Bombyx mori*, is a suitable hydrogel candidate material for bioapplications due to its biocompatibility, biodegradation and easy processability.[3,4] RSF hydrogels could be prepared by inducing β-sheet formation in RSF aqueous solutions *via* several triggers such as temperature,[5] pH,[6] metal ions,[7] sonication,[8] vortexing[9] surfactants[10,11] or by chemical crosslinking of RSF.[12] However, the RSF hydrogels generally exhibit weak mechanical properties and lack of functionality, which limits their use in various biomedical applications.

Many efforts have been employed to improve the mechanical properties of RSF hydrogels, including micro-nano fiber reinforcing,[13,14] binary-solvent-induced conformation transition (BSICT),[15] low temperature gelation technique/cryogelation.[16,17], dual-crosslinking[18] and double network concept.[19–21] Among them, double network concept has been proved to be a more effective strategy. Double network hydrogels (DN hydrogels) usually consist of two single networks, the first network is rigid and brittle, and the second network is soft and ductile. By increasing and enhancing covalent or non-covalent interactions within and between the two networks, their combined networks can be strong and tough.[22,23] For example, Chen *et al.* developed RSF/HPAAm DN hydrogels, which combined an H-bond-stabilized SF as first network and a hydrophobically associated network of polyacrylamide (HPAAm) as the second network. the RSF/HPAAm DN hydrogels exhibited high strength (1.17 MPa) and high toughness (11.75 MJ m^3).[19] Zhao and co-workers modified Chen's method to enhance the stability of as-prepared DN hydrogels by introducing SDS post-immersion process, but the mechanical strength of the equilibrium state DN hydrogels were decreased.[20] Although the above works improve the mechanical properties of RSF DN hydrogels, the use of SDS surfactants may hinder their further application as biomaterials, especially in cases where bioactive molecules and cells need to be encapsulated.

The silk fibroin molecule consists of repetitive hydrophobic crystalline regions (GAGAGS) interspersed with non-repetitive hydrophilic amorphous regions.[20–23] There are 12 hydrophobic crystalline domains distributed in 11 hydrophilic amorphous domains and 2 hydrophilic terminals (N- and C-terminal), which make silk fibroin a natural amphiphilic multiblock copolymer.[24–26]. On account of this distinctive structure, the surface activity of silk fibroin at the oil/water emulsions have

College of Materials Science and Engineering, Taiyuan University of Technology, Taiyuan, 030024, China. E-mail: zhujingxin@tyut.edu.cn

† Electronic supplementary information (ESI) available: Preparation of regenerated silk fibroin (RSF) solutions, the text of emulsifying ability of pure silk fibroin and self-healing capability of the DN gels. See https://doi.org/10.1039/d2ra00954d

been explored. Shao's team reported that silk fibroin could prevent droplet coalescence and facilitate oil/water mixture to form a stable emulsion.[27] Recently, Maxwell *et al.*[28] found that silk fibroin could be combination with sugar surfactants to develop high performance cosurfactant system for cosmetic formulations. Thus, it may be a good choice to use RSF's amphiphilicity and excellent biocompatibility as a surfactant to stabilize the physical cross-linking network formed by hydrophobic interactions.

The purpose of this study was to developed non-toxicity RSF-based hydrogels with good mechanical properties, self-healing and electrical conductivity *via* the DN strategy. RSF/S-PAAm/C18 DN gels were prepared by free radical polymerization ion one pot method. RSF/S-PAAm/C18 DN gels were full physical DN gels, consisting of a sonication-induced β-sheet physically cross-linked RSF/S gel as the first network and a hydrophobically associated polyacrylamide/stearyl methacrylate (PAAm/C18) gel as the second network. Especially, in preparation, the monodisperse micelles, which formed by a cosurfactant RSF-sugar and hydrophobic monomer stearoyl methacrylate (C18M), were used as the physical cross-linking point for PAAm/C18 network, while the addition of calcium ions was expected to increase the self-healing and electrical conductivity of the DN gels. After testing, it was shown that the design RSF-based double network gels showed large extensibility, high tensile strength, rapid self-recovery, satisfactory self-healing capability and electrical conductivity. The newly DN hydrogels has great potential in applications, such as tissue engineering, biosensors and artificial electronic skin.

Results and discussion

SF/CG/C18M O/W emulsions

Silk fibroin (SF) has good amphiphilic and surface activity, its molecular chain could diffuse from aqueous solution to the water–oil interface to prevent droplet aggregation and form a stable emulsion.[26] Proteins tend to achieve higher surface activity at lower concentrations[29,30] According to our preliminary results (ESI Table S1†), 2% SF solution showed good emulsification and stability for stearoyl methacrylate (C18M).

Caprylyl glucoside (CG), a green natural surfactant,[31,32] is expected to enhance the surface activity and emulsification stability of SF.[27] Therefore, we mixed 2% SF and CG in different proportions, added C18M (0.0746 mM ml^{-1}), and then treated with low energy ultrasound to promote emulsification and micelles formation. The particle size and zeta potential of SF/CG/C18M emulsions were tested by a particle size analyzer, and the results are shown in Table 1. When C18M was emulsified using SF, the average particle size of micelles was 806 nm, and the zeta potential was −18.2 mV. With the addition of CG, the particle size of the micelles decreased, and the distribution was narrow (PDI, 0.2), meanwhile, the absolute value of zeta potential also increased, indicating that SF and CG had a synergistic effect on the emulsification of C18M. Fig. 1 shows the appearance and particle size distribution of SF/CG/C18M emulsion when RSF : CG was 100 : 20. The average micelles size of the emulsion was 355 nm, and the zeta potential was −37.1 mV, indicating that the emulsion was in good stability.

Table 1 Micelles size, dispersion index and surface charge in C18M emulsion stabilized by different composition of silk fibroin (SF) and capryl glucoside (CG)

C18M density (mM ml^{-1})	SF : CG (wt : wt)	Droplet size (nm)	PDI	Zeta potential (mV)
0.0746	100 : 0	805.9	0.220	−18.2
0.0746	100 : 10	358.4	0.201	−30.7
0.0746	100 : 20	355.2	0.203	−37.1

Synthesis of RSF/S-PAAm/C18 DN gels

RSF/S-PAAm/C18 DN gels were synthesized by the free radical polymerization using one-pot method with different composition (Table 2) Briefly, 5% RSF- sonicated solution containing β-sheet nuclei, 35% RSF solution, and SF/CG/C18M emulsions should be prepared primarily, and other reagents including AAm (monomer), APS (initiator) and $CaCl_2$ were then add to this solution. After all the chemicals were dissolved, the solution was transferred into a home-made silastic mould. The DN hydrogel was obtained after polymerization at 37 °C for 12 h. In the DN gel, RSF/S first networks was formed by sonication-induced the conformation transition of RSF from random coil to β-sheet, and PAAm chains penetrated the network to form the hydrophobically associated PAAm/C18-second network. The RSF/S-PAAm/C18 DN gels were all physically cross-linked network. Moreover, the presence of Ca^{2+} ions in the DN gels could act as a conductor to improve the conductivity and self-healing properties of the DN gels. Schematic diagram of preparation RSF/S-PAAm/C18 DN gel is shown in Fig. 2.

FTIR measurement

FTIR was performed to characterize the structural information of RSF/S SN gel, PAAm/C18 SN gel, and RSF/S-PAAm/C18 DN gel, as displayed in Fig. 3. The spectrum of RSF/S SN gel shown typical peaks at 1627 and 1521 cm^{-1}, assigned to amide I and amide II of the β-sheet conformation in RSF proteins.[33,34] This

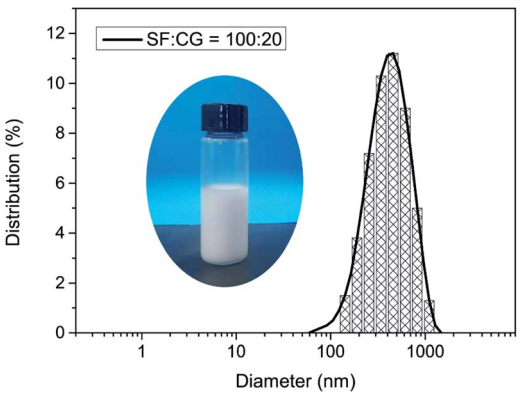

Fig. 1 Digital photo and particle size distribution of stabilized emulsion when SF : CG = 100 : 20 (wt : wt).

Table 2 The composition of RSF/S-PAAm/C18 DN hydrogels

Samples	β-Sheet nuclei (g ml^{-1})	Ca^{2+} (mM ml^{-1})	RSF (g ml^{-1})	AAm (mM ml^{-1})	C18M (mM ml^{-1})	APS (mM ml^{-1})
PAAm/C18	0	0	2	3.770	0.0746	0.0679
$RSF_{4.3}$/S-PAAm/C18	0.078	0.405	4.3	3.770	0.0746	0.0679
$RSF_{6.1}$/S-PAAm/C18	0.144	0.748	6.1	3.770	0.0746	0.0679
$RSF_{7.7}$/S-PAAm/C18	0.200	1.036	7.7	3.770	0.0746	0.0679
$RSF_{8.9}$/S-PAAm/C18	0.240	1.289	8.9	3.770	0.0746	0.0679

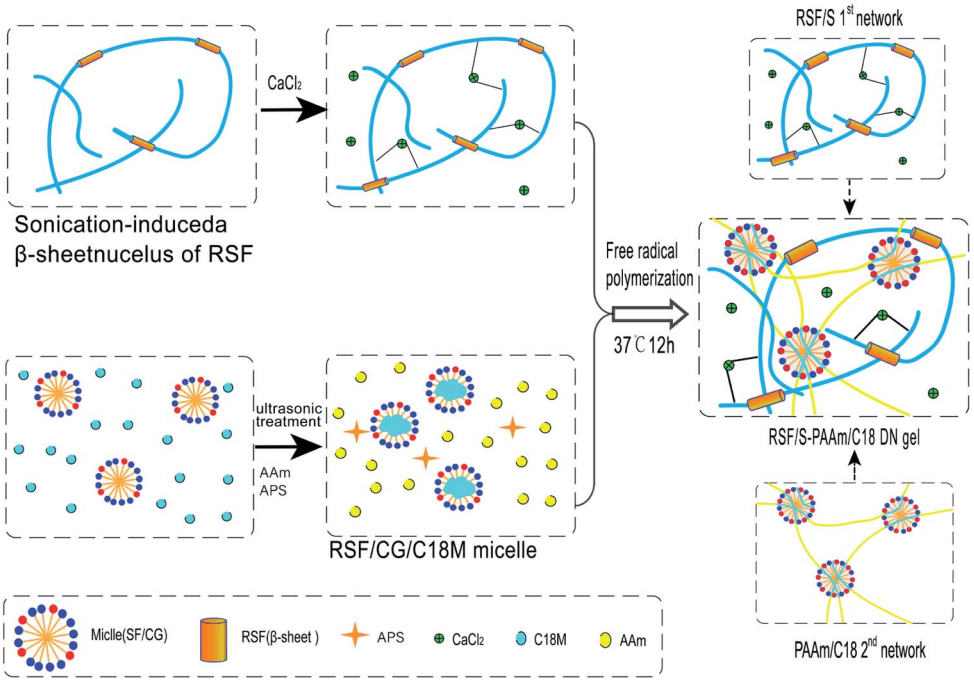

Fig. 2 Schematic diagram of preparation RSF/S-PAAm/C18 double network gels.

indicated that ultrasound-induced β-sheet physical crosslinks network were formed in RSF/S hydrogel. For PAAm/C18 SN gel, the peak at 1648 cm^{-1} was due to the amide band of the amide group of PAAm (>C=O stretching vibration), In the case of RSF_x/S-PAAm/C18 DN hydrogels, the peak at 1637 cm^{-1} was the absorbance of the Amide I of RSF chains overlaps with amide group of PAAm, while the peak at 1521 cm^{-1} was the amide II of RSF, indicating the presence of β-sheet conformation in the DN hydrogels. The large absorbance in 3429–3826 cm^{-1} corresponding to associated hydrogen bonds also indicated a mass of intra- and intermolecular interactions within single or double networks of RSF_x/S, PAAm/C18 and RSF_x/S-PAAm/C18 DN gels.

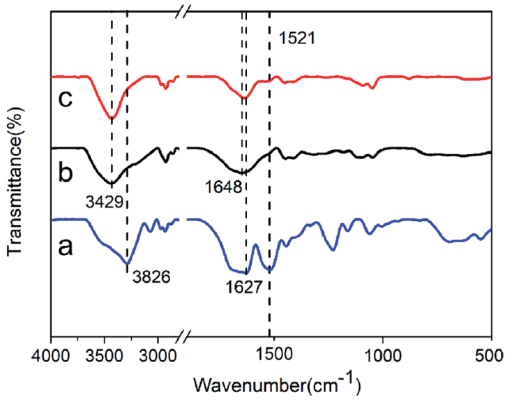

Fig. 3 FTIR spectra of pure RSF_x/S gel (a), PAAm/C18 SN gel (b) and. $RSF_{7.7}$/S-PAAm/C18 DN gel (c).

Morphologies of RSF/S-PAAm/C18 DN gels

Scanning Electron Microscopic (SEM) was used to observe the cross-sectional morphologies of RSF_x/S-PAAm/C18 DN gels with different RSF content at 4.3, 6.1, 7.7, 8.9 (wt/v)% respectively, are represented by curves a, b, c, and d in Fig. 4. It can be seen that uniform pore distribution throughout the matrices and no visible phase separation. The pores were open, interconnected with well defined boundaries. With the increase of RSF content from 4.3 to 8.9 (wt/v)%, the pore size of the gels decreased from 12 ± 2 μm to 4 ± 2 μm, and the boundary wall between the pores became thinner. This may be because with the increase of RSF content, the density of polymer chains increased and the water

content decreased, resulting in smaller ice crystals and an increase in the number of pores per unit area.

Swelling behavior analysis

Water absorbed by the DN hydrogels was monitored constantly for an extended period of time till equilibrium was achieved. Swelling ratios of RSF_x/S-PAAm/C18 DN hydrogels at 4 °C were calculated by using eqn (1) and plotted as a function of DN hydrogels composition in Fig. 5A. The hydrogels swelled rapidly in water and attained equilibrium within 72 hours. The swelling ratio was found to be dependent on the content of first RSF/S network. With increase in RSF/S percentage, the swelling ratio of the DN hydrogels decreased (Fig. 5B). $RSF_{4.3}$/S-PAAm/C18 DN hydrogels showed high equilibrium water content of 1370%, compared to 650% in case of $RSF_{8.9}$/S-PAAm/C18 DN hydrogels. This was probably due to larger diameter pores and low the density of physical cross-linking point (β-sheet domain) in the $RSF_{4.3}$/S-PAAm/C18 DN gels, and supported by the fact that the higher the crosslinking degree of the gel, the lower the swelling ratio of matrix in water.

Mechanical properties

The mechanical properties of the RSF_x/S-PAAm/C18 DN hydrogels with different contents of RSF were firstly investigated, as shown in Fig. 6A. It can be seen that the hydrogels had good ductility, the PAAm/C18 SN gel could be stretched more than 2000% due to its unique micellar structure as a crosslinking point. Compared with PAAm/C18 SN gel, RSF_x/S-PAAm/C18 DN gels had better mechanical properties. The maximum stress was 0.3 ± 0.03 MPa, nearly 2.7 times that of PAAm/C18 SN gel, and the maximum elongation still reached 1560%. This is due to the synergistic enhancement of double networks through the combination of PAAm/C18 flexible single network and RSF_x/S hard single network. When stretched of the DN gels, the hydrogen bond between DN network was first destroyed, meanwhile, the PAAm/C18 flexible network was dispersed and consumed a lot of energy, which protected RSF_x/S network and made the gel obtain ductility and toughness.[35] In addition, it was found that the work of tension of the DN gels was closely related to the content of RSF in the gels, the work of tension was calculated and was showed in Fig. 6B. Then, it can be seen that the toughness of the RSF_x-PAAm/C18 DN gels was higher than that of PAAm/C18 SN gel, and the work of tension of the DN gels increased when the content of RSF increased from 6.1 to 7.7% (wt/v)%, but that of the DN gels decreased when the content of RSF increased from 7.7 to 8.9% (wt/v)%. The reason is that although the combination of double networks could improve the mechanical properties of the DN gels, but when the RSF_x/S hard network content was too high, the PAAm/C18 soft network could not disperse the energy well, so the DN gel showed brittleness and reduced the toughness. On the other hand, the elastic modulus of the DN hydrogels were weak and to be like human skin.[36] Therefore, at the optimal conditions, such as the content of RSF was 7.7% (wt/v)%, the $RSF_{7.7}$/S-PAAM/C18 DN hydrogel showed the maximum the work of tension (1.78 MJ m^3), high stretch (1400%) and elastic modulus (0.081 MPa).

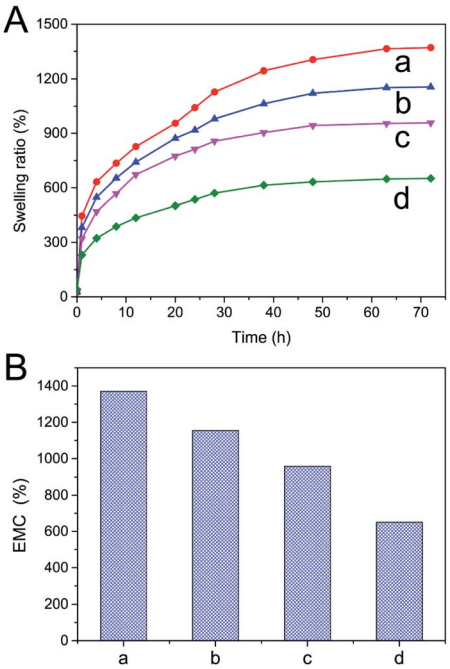

Fig. 5 (A) Swelling ratio of DN hydrogels in water at 4 °C against time, $RSF_{4.3}$/S-PAAm/C18 DN hydrogels (a), $RSF_{6.1}$/S-PAAm/C18 DN hydrogels (b), $RSF_{7.7}$/S-PAAm/C18 DN hydrogels (c) and $RSF_{8.9}$/S-PAAm/C18 DN hydrogels (d). (B) Summary of equilibrium water content of the DN hydrogels after 72 h of swelling.

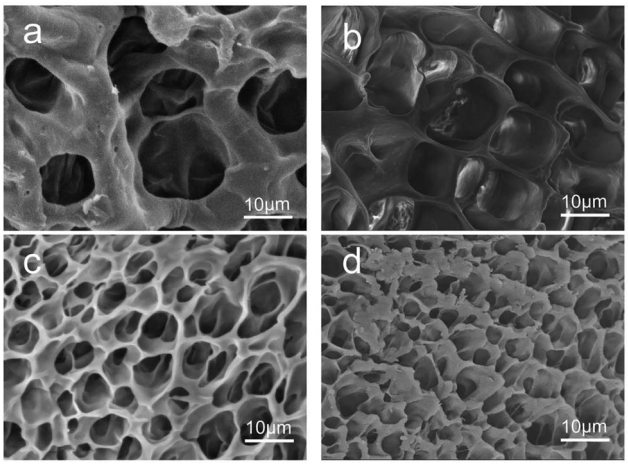

Fig. 4 Cross-sectional morphologies of $RSF_{4.3}$/S-PAAm/C18 DN gel (a), $RSF_{6.1}$/S-PAAm/C18 DN gel (b), $RSF_{7.7}$/S-PAAm/C18 DN gel (c), $RSF_{8.9}$/S-PAAm/C18 (DN gel (d)).

Recovery properties

In order to evaluate recovery properties and dissipation energy of the $RSF_{7.7}$/S-PAAM/C18 DN hydrogel, the loading–unloading cyclic tests with strain ranging from 100% to 800% were performed and the results are shown in Fig. 7. It can be seen in Fig. 7A that hysteresis loop of the DN gel was gradually obvious when the tensile strain increased from 100% to 800%, indicating that the hydrogels dissipated energy efficiently. The

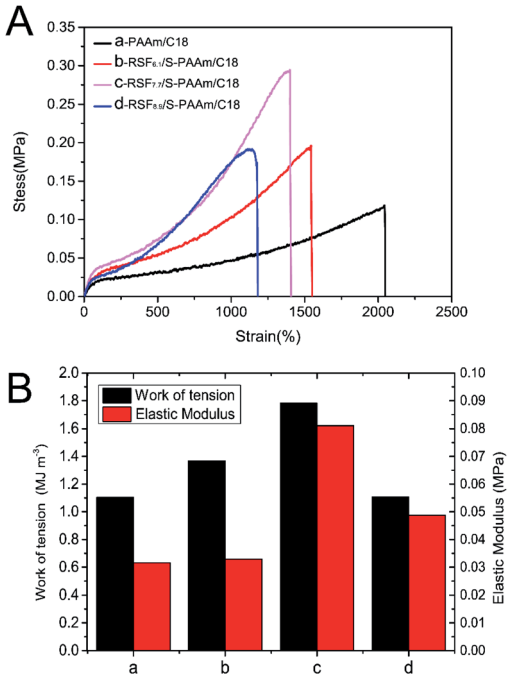

Fig. 6 (A) Tensile stress–strain curves of the PAAm/C18 SN hydrogel (a) and RSF_x/S-PAAm/C18 DN hydrogels with varied RSF contents: $RSF_{6.1}$/S-PAAm/C18 hydrogel (b), $RSF_{7.7}$/S-PAAm/C18 hydrogel (c), $RSF_{8.9}$/S-PAAm/C18 hydrogel (d). (B) Summary of toughness and elastic modulus of RSF_x/S-PAAm/C18 DN hydrogels.

presence of intra- and intermolecular hydrogen bonds in RSF/S network as well as hydrophobic interaction in PAAm/C18 network contributed to the large energy dissipation by means of dissociation or decrosslinking.[37] When the DN gel was subjected to continuous cyclic stretching, with the dissipation energy in the range of 0.013–0.09 MJ m^{-3} (Fig. 7C, black). In addition, plastic deformation was appeared and increased from 40% to 260% after loading and unloading when the tensile strain increased from 100% to 800% (Fig. 7D, blue), illustrating the viscoelastic behaviour of the DN gel. In order to further evaluate the self-recovery performance of the DN gel at room temperature, we conducted loading and unloading cyclic tensile tests with different strain at an interval of 60 seconds, the results are shown in Fig. 7B. It was observed that the recovered DN hydrogels achieved higher stress than its without interval stress. This phenomenon was ascribed to that re-association or re-crosslinking of two physical networks allowed their optimal reorganization for repairing damaged networks.[38,39] Moreover, with 60 seconds interval maximum energy dissipated of the recovered the DN hydrogels increase to 0.10 MJ m^{-3}, compared with 0.09 MJ m^{-3} for the without interval samples (Fig. 7C), This is because the energy dissipated in irreparable plastic deformation was decreased as the sacrificial bond in DN network was repaired. Significant reduction of plastic deformation can be seen in the cyclic stretching process with an interval of 60 seconds, the maximum deformation was 121 ± 5%. Therefore, the DN gel can be reused at fewer rest intervals, which makes it advantageous in the field of wearable devices that require low residual strain and fast self-recovery ability.

Self-healing properties

The dynamic characteristics of hydrogen bond and hydrophobic interaction endowed the DN hydrogel with good self-healing ability. As shown in Fig. 8A, the stained (rhodamine B) and unstained of the DN gel samples were cut into two pieces

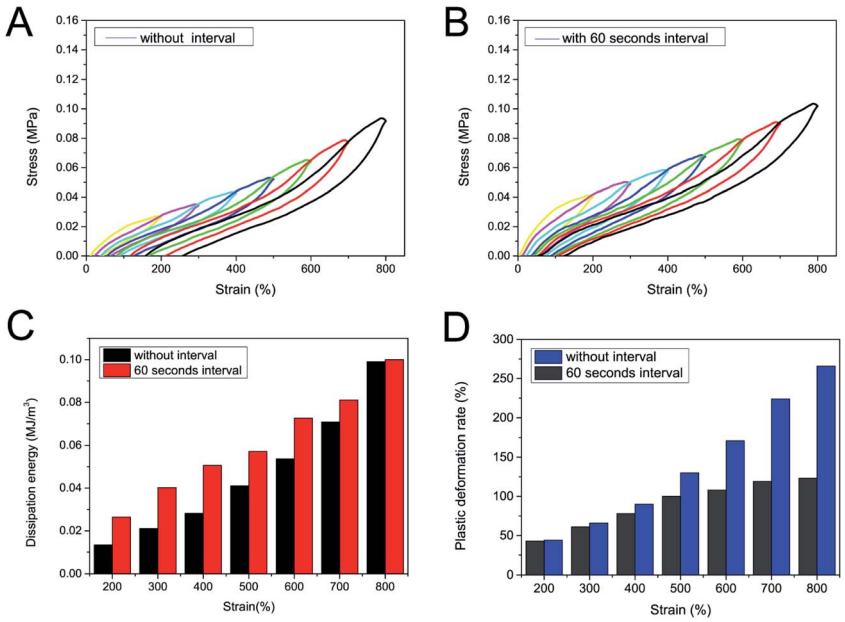

Fig. 7 Loading–unloading cyclic tests of the $RSF_{7.7}$/S-PAAm/C18 DN hydrogels at the strains from 100% to 800%. (A) without interval, (B) with 60 seconds interval. (C) Dissipation energy of the $RSF_{7.7}$/S-PAAM/C18 DN hydrogels at different strains (100–800%) without interval and 60 seconds interval. (D) Plastic deformation of the $RSF_{7.7}$/S-PAAM/C18 DN hydrogels at different strains (100–800%) without interval and 60 seconds interval.

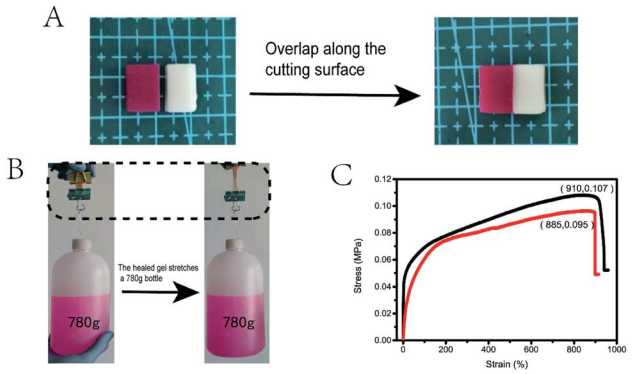

Fig. 8 (A) Rhodamine B-stained gel and unstained gel were cut into two pieces (10 mm × 7 mm × 15 mm) and fitted along the incision, (B) the self-healing $RSF_{7.7}$/S-PAAm/C18 DN hydrogel pulled up a 780 g water bottle, (C) stretching curve of $RSF_{7.7}$/S-PAAm/C18 DN hydrogel before and after self-healing.

of 10 mm × 7 mm × 15 mm. The incisions were put together to let repair for 12 h in an incubator at 37 °C. Tensile test was conducted to compare the properties of the DN gels with different RSF and Ca^{2+} contents of before and after self-healing, and it was found that $RSF_{7.7}$/S-PAAM/C18 gel had the best self-healing performance (Fig. 8C), with the self-healing rate of stress up to 88% ± 2%, and the self-healing rate of strain up to 95% ± 2% (the self-healing performance of other composition DN gels are shown in ESI Fig. S1†). Using the healed hydrogel to pull up the actual object, it could pull up a bottle with 750 ml water and 30 g of its own weight (Fig. 8B). The self-healing mainly derived from the reversibility of hydrophobic interactions and hydrogen bonds between RSF and PAAm chains. As shown in Fig. 9, when the two cutting-off hydrogels were brought into together at 37 °C, the hydrophobic interactions in C18 micelles blocks were repaired, meanwhile, the RSF and PAAm chains diffused across the interface from both sides to reform the hydrogen bonds in the bulk.[40] Moreover, Ca^{2+} ion in the gel could improve the self-healing ability because of the electrostatic interaction between Ca^{2+} ion and the carboxyl group in chains of RSF.[41]

Ionic conductivity of $RSF_{7.7}$/S-PAAm/C18 DN gels

Considering that $RSF_{7.7}$/S-PAAm/C18 DN gel contained an amount of free calcium ions, it was expected that the gels could exhibit ionic conductivity. The conductivity test was carried out under 1 V voltage. It can be seen that the conductivity of the gel remained stable after 600 s and the current gradually approached 1.1 mA (Fig. 10 B), the slight decreases of the current might be due to electrolysis of the water. The calculated conductivity was 0.12 $S \cdot m^{-1}$, showing good conductivity. The resistance change of the gel with strain was also measured, it was found that with the tensile deformation of the gel increased, the resistance of the gel increased, and the change of the resistance was a nearly smooth curve. After 500% strain, the resistance increased more than 2.5 times (Fig. 10C), which proved that the gel had good sensitivity and adjustability. As shown in Fig. 10A, the DN gel in the closed circuit was connected to a light-emitting diode (LED), which successfully lights up after the power was turned on, when the gel was stretched, the brightness of the diodes decreased, but remained stable for some time. Therefore, the hydrogel has a good application prospect in the field of flexible sensors.

Experimental

Materials

Silk cocoon purchased from Zhejiang, China. Ammonium persulfate (APS, 99%), acrylamide (AAm, 99%), purchased from Sinopharm Chemical Reagent Co., Ltd. Stearoyl methacrylate (C18M, 99%), capryl glucoside (CG, 99%), purchased from Macklin, lithium bromide (LiBr, 99%) was purchased from Shanghai Zhongli Industry Co., LTD., All other reagents including $CaCl_2$, Na_2CO_3, rhodamine B, were of analytical grade, and used as received without further purification.

Preparation of SF/CG/C18M micelle emulsion

2% (wt/v) SF solution (prepared according to the procedure in ESI†) and 50% (wt/v) capryl glucoside were mixed into 100 : 0, 100 : 10 and 100 : 20 (wt : wt) solutions at different volume ratios. After stirring in a 25 ml glass bottle for 10 minutes, C18M (0.0746 mM ml^{-1}) was added. The mixed solution was sonicated with a XO-650D (Nanjing Xianou Instrument Manufacturing Co., Ltd.) for one minute at 25% power to promote the formation of stable emulsion, which containing SF/CG/C18M micelles.

Preparation of sonication-induced β-sheet RSF/S SN hydrogel

5% RSF(6 ml) was sonicated with a XO-650D for six minutes at 45% power to induce the nucleation of β-sheets in the solution.

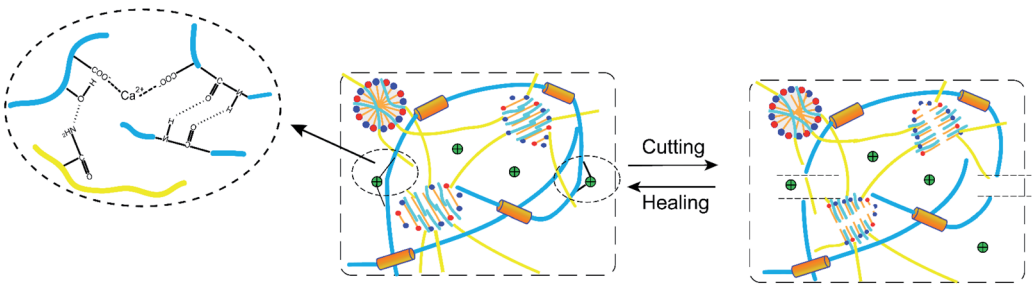

Fig. 9 Self-healing mechanism schematic diagram of RSF_x/S-PAAM/C18 DN hydrogel.

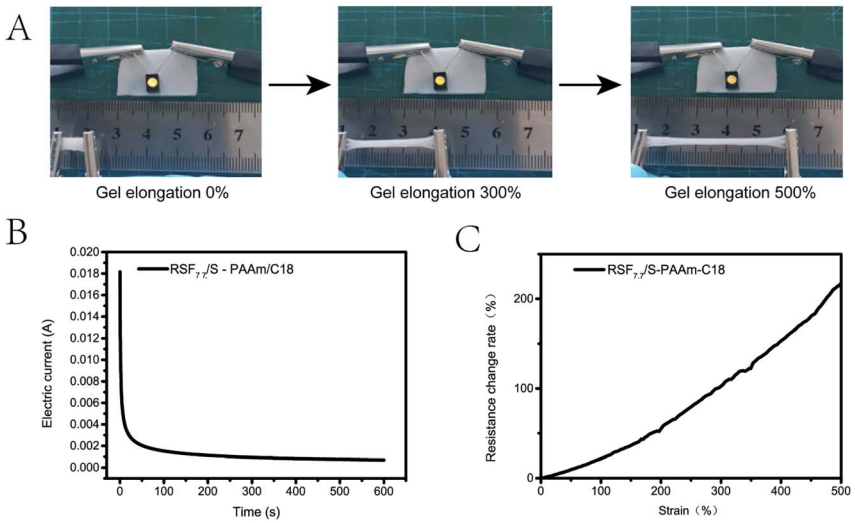

Fig. 10 (A) Schematic diagram of different elongation of $RSF_{7.7}$/S – PAAm/C18 DN gel in a diode conductive loop. (B) Current-time curves of $RSF_{7.7}$/S – PAAm/C18 DN gel at 1V voltage. (C) Resistance-strain curve as the gel extends.

Then the β-sheet nuclei solution was used to mix with 35 wt% RSF solution in a certain proportion at 1 : 4 (v/v) and incubated at 37 °C for 12 h to promote the growth of β-sheets and form the RSF/S physical network hydrogel.

Preparation of RSF/S-PAAm/C18 DN hydrogel

The RSF/S-PAAm/C18 DN hydrogels were prepared by a one-pot method. AAm (3.770 mM ml^{-1}), APS (0.0679 mM ml^{-1}, 1.8% mol% relative to AAm) and 10 ml SF/CG/C18M micelle emulsion, were added to a beaker under stirring for 10 min, then various concentrations of RSF solutions containing a constant concentration of β-sheets nuclei (88% (wt : wt) relative to $CaCl_2$) and $CaCl_2$ were added and mixed, respectively, the samples were named as RSF_x/S-PAAm/C18, RSF_x, in which x represent the concentration of RSF in the DN hydrogel. For test sample, the solutions were transferred into a square mould that was prepared by sandwiching 2 mm silicone rubber between two glass plate, and the incubated at 37 °C for 12 h to form the hydrogels.

Characterization and testing

The average size and surface charge of SF/CG/C18M micelles were measured from the stable C18M emulsion by using a Zetasizer Nano ZS90 particle size analyzer (MALVERN, England). FT-IR Samples were recorded on a TENSOR II Spectrometer (BRUKER, Germany) with a resolution of 4 cm^{-1} in the sample. The cross-sectional morphologies of RSF_x/S-PAAm/C18 DN gel were carried out using a Mira 3 scanning electron microscopy (SEM) (TESCAN, Czech). Swelling properties were studied using conventional gravimetric procedure.[42] The hydrogel samples were swelled in deionized water 12 hours and frozen at liquid nitrogen followed by lyophilization. The swelling behaviour of the samples was determined by immersing the completely dried hydrogel samples in deionized water at 4 °C. The swelling ratio (SR) was calculated by the following formula:

$$SR = (M_t - M_0)/M_0 \times 100 \quad (1)$$

where M_t is the mass of the swollen gel at time t, and M_0 is the mass of the dry gel at time 0.

The quality of the gel was tested constantly, all the gels have reached swelling equilibrium after 72 hours, equilibrium water content (EWC) of the gel was calculated by the following formula:

$$EWC = (M_e - M_0)/M_0 \times 100 \quad (2)$$

where M_e is the mass of the gel after attainment of equilibrium at 72 h, M_0 is the mass of the dry gel at time 0.

All mechanical tests were carried out on a universal tensile testing machine (UTM4304X, Shenzhen) at room temperature and 35% humidity. The samples with a thickness of 2 mm were chop into rectangular or dumbbell-shaped shape (2 mm × 2 mm × 12 mm) to measure tensile properties. The rate of extension was fixed at 50 mm min^{-1} for tensile tests and 50 mm min^{-1} for loading-unloading tests. The work of tension was calculated from the slope over 0–10% of strain ratio of stress–strain curves. The work of tension (toughness) was calculated from the area below the tensile stress–strain curve. Energy dissipation was calculated from the area of the hysteresis loop. All the gels were measured for at least 5 separate tests; the tensile properties were denoted by average values with deviations. The conductivity of the hydrogel was tested at an electrochemical workstation (CHI600E, Shanghai). The samples were tested on a column with a diameter of 30 mm and a height of 10 mm (in original wet state). The current–time curves of the hydrogel were recorded at a constant pressure of 1 V at room temperature. The conductivity (σ) was calculated by the following formula:

$$s = IL/US \quad (3)$$

where σ ($S \cdot m^{-1}$) is the conductivity of the hydrogel, U (V) is the voltage at both ends of hydrogel; I (A) is the current through the hydrogel; L (m) is the length of hydrogel sample and S (m^2) is the cross-sectional area of hydrogel sample.

The rate of resistance change with gel elongation was measured by tensile testing machine (ZQ-990B) and digit multi meter (TH1963) at room temperature. The test sample is rectangular sample, 30 mm long, 10 mm wide, 2 mm thick. The relative resistance change rate (α) was calculated by the following formula:

$$\alpha = \Delta R/R_0 \quad (4)$$

R_0 (Ω) is the initial resistance of hydrogel before stretching. And ΔR (Ω) is the resistance change during hydrogel stretching.

Conclusion

In summary, we have synthesized a green full physical crosslinked double-network RSF-based hydrogel, consisting of a sonication induced β-sheet physically crosslinked RSF/S gel as the first network and a hydrophobically associated PAAm/C18 gel as the second network. In particular, the cross-linking points of the second network were micelles formed by emulsifying the hydrophobic monomer C18M with SF and capryl glucoside co-surfactant. The reversible dynamic bonds provided good self-healing ability and effective dissipative energy mechanism for the hydrogel, while the addition of calcium ions improved the self-healing and electrical conductivity of the hydrogel. The mechanical performances of the hydrogels could be adjusted by changing the content of RSF. At optimal conditions, the RSF/S-PAAm/C18 DN gels exhibited large extensibility (1400%), and high tensile strength (0.3 MPa). Moreover, the self-healing capability and electrical conductivity of the DN hydrogel could reach nearly 90% and 0.12 $S \cdot m^{-1}$, respectively. Such physically interacted DN hydrogels, combination of stretchable, self-recovery self-healing, conductivity and biocompatible, is expected to be applied in various fields such as tissue engineering, biosensors and artificial electronic skin.

Author contributions

Tao Fang: methodology, investigation, data curation, writing-original draft, Jingxin Zhu, conceptualization, validation, writing – review & editing, Shuai Xu, Lan Jia: participating in experiments, data curation, Yanlong Ma: validation, funding acquisition.

Conflicts of interest

The authors declare there is no conflict of interest.

Acknowledgements

The authors acknowledge financial support from the Natural Science Foundation of Shanxi Province, China (201801D121102).

Notes and references

1 P. Calvert, *Adv. Mater.*, 2009, **21**, 743–756.
2 H. Yu, X. Hao, C. Zhang, S. Zheng, M. Du, S. Liang, Z. Wu and Q. Zheng, *Small*, 2021, **17**, 2103836.
3 S. Fan, J. Chen, Z. Gu, X. Yao and Y. Zhang, *Acta Polym. Sin.*, 2021, **52**, 20.
4 J. Zhu, Y. Zhang, H. Shao and X. Hu, *Polymer*, 2008, **49**, 2880–2885.
5 A. Matsumoto, J. Chen, A. L. Collette, U.-J. Kim, G. H. Altman, P. Cebe and D. L. Kaplan, *J. Phys. Chem. B*, 2006, **110**, 21630–21638.
6 Y. Yang, Z. Shao and X. Chen, *Acta Chim. Sin.*, 2006, **64**, 1730.
7 U.-J. Kim, J. Park, C. Li, H.-J. Jin, R. Valluzzi and D. L. Kaplan, *Biomacromolecules*, 2004, **5**, 786–792.
8 X. Wang, J. A. Kluge, G. G. Leisk and D. L. Kaplan, *Biomaterials*, 2008, **29**, 1054–1064.
9 T. Yucel, P. Cebe and D. L. Kaplan, *Biophys. J.*, 2009, **97**, 2044–2050.
10 X. Wu, J. Hou, M. Li, J. Wang, D. L. Kaplan and S. Lu, *Acta Biomater.*, 2012, **8**, 2185–2192.
11 S. Sun, F. Zhang, S. Zhang, T. Xing and S. Lu, *Biotechnology*, 2013, **12**, 128.
12 I. Karakutuk, F. Ak and O. Okay, *Biomacromolecules*, 2012, **13**, 1122–1128.
13 S. Yodmuang, S. L. McNamara, A. B. Nover, B. B. Mandal, M. Agarwal, T.-A. N. Kelly, P.-h. G. Chao, C. Hung, D. L. Kaplan and G. Vunjak-Novakovic, *Acta Biomater.*, 2015, **11**, 27–36.
14 J. Ming, M. Li, Y. Han, Y. Chen, H. Li, B. Zuo and F. Pan, *Mater. Sci. Eng., C*, 2016, **59**, 185–192.
15 Z. Zhu, S. Ling, J. Yeo, S. Zhao, L. Tozzi, M. J. Buehler, F. Omenetto, C. Li and D. L. Kaplan, *Adv. Funct. Mater.*, 2018, **28**, 1704757.
16 B. Yetiskin and O. Okay, *Polymer*, 2017, **112**, 61–70.
17 B. Yetiskin and O. Okay, *Int. J. Biol. Macromol.*, 2019, **122**, 1279–1289.
18 Z. Li, Z. Zheng, Y. Yang, G. Fang, J. Yao, Z. Shao and X. Chen, *ACS Sustainable Chem. Eng.*, 2016, **4**, 1500–1506.
19 F. Chen, S. Lu, L. Zhu, Z. Tang, Q. Wang, G. Qin, J. Yang, G. Sun, Q. Zhang and Q. Chen, *J. Mater. Chem. B*, 2019, **7**, 1708–1715.
20 Y. Zhao, J. Guan and S. J. Wu, *Macromol. Rapid Commun.*, 2019, **40**, 1900389.
21 D. Gong, Q. Lin, Z. Shao, X. Chen and Y. Yang, *RSC Adv.*, 2020, **10**, 27225–27234.
22 Q. Chen, H. Chen, L. Zhu and J. Zheng, *J. Mater. Chem. B*, 2015, **3**, 3654–3676.
23 Y. Zhao, Z. Zhu, J. Guan and S. Wu, *Acta Biomater.*, 2021, **125**, 57–71.

24 C. Zhou, F. Confalonieri, M. Jacquet, R. Perasso, Z. Li and J. Janin, *Proteins: Struct., Funct., Bioinf.*, 2001, **44**, 119–122.
25 F. Braun and C. Viney, *Int. J. Biol. Macromol.*, 2003, **32**, 59–65.
26 S.-W. Ha, H. S. Gracz, A. E. Tonelli and S. M. Hudson, *Biomacromolecules*, 2005, **6**, 2563–2569.
27 W. Peng, L. Wang, X. Qiao, Z. Shao and K. Sun, *Chem. J. Chin. Univ.*, 2015, **36**, 1012–1018.
28 R. Maxwell, M. C. Costache, A. Giarrosso, C. Bosques and S. Amin, *Int. J. Cosmet. Sci.*, 2021, **43**, 68–77.
29 K. Sze-Tao and S. Sathe, *Food Chem.*, 2000, **69**, 153–160.
30 Q. Guo and T. Mu, *Food Hydrocolloids*, 2011, **25**, 98–106.
31 S. Matsumura, K. Imai, S. Yoshikawa, K. Kawada and T. Uchibor, *J. Am. Oil Chem. Soc.*, 1990, **67**, 996–1001.
32 K. Holmberg, *Curr. Opin. Colloid Interface Sci.*, 2001, **6**, 148–159.
33 S. A. Fossey, G. Némethy, K. D. Gibson and H. A. Scheraga, *Biopolymers: Original Research on Biomolecules*, 1991, **31**, 1529–1541.
34 W. Zhou, X. Chen and Z. Shao, *Prog. Chem.*, 2006, **18**, 1514–1522.
35 S. Lin, X. Liu, J. Liu, H. Yuk, H.-C. Loh, G. A. Parada, C. Settens, J. Song, A. Masic and G. H. McKinley, *Sci. Adv.*, 2019, **5**, eaau8528.
36 H. Ding, X. Liang, Q. Wang, M. Wang, Z. Li and G. Sun, *Carbohydr. Polym.*, 2020, **248**, 116797.
37 A. Pourjavadi, M. Tavakolizadeh, S. H. Hosseini, N. Rabiee and M. Bagherzadeh, *J. Polym. Sci.*, 2020, **58**, 2062–2073.
38 Y. Yang, X. Wang, F. Yang, H. Shen and D. Wu, *Adv. Mater.*, 2016, **28**, 7178–7184.
39 Y. Huang, L. Xiao, J. Zhou, T. Liu, Y. Yan, S. Long and X. Li, *Adv. Funct. Mater.*, 2021, **31**, 2103917.
40 G. Akay, A. Hassan-Raeisi, D. C. Tuncaboylu, N. Orakdogen, S. Abdurrahmanoglu, W. Oppermann and O. Okay, *Soft Matter*, 2013, **9**, 2254–2261.
41 J. W. Seo, H. Kim, K. Kim, S. Q. Choi and H. J. Lee, *Adv. Funct. Mater.*, 2018, **28**, 1800802.
42 B. Vázquez, J. San Roman, C. Peniche and M. E. Cohen, *Macromolecules*, 1997, **30**, 8440–8446.